$K\alpha$ and $K\beta$ x-ray emission spectra of copper

M. Deutsch[1], G. Hölzer[2], J. Härtwig[3], J. Wolf[4], M. Fritsch[2] and E. Förster[2]
[1]*Physics Department, Bar-Ilan University, Ramat-Gan 52900, Israel*
[2]*Max-Planck-Arbeitsgruppe "Röntgenoptik" an der Friedrich-Schiller-Universität Jena, Max-Wien-Platz 1, D-07743 Jena, Germany*
[3]*European Synchrotron Radiation Facility, Boîte Postal 220, F-38043 Grenoble Cedex, France*
[4]*Institut für Optik und Quantenelektronik, Friedrich-Schiller-Universität Jena, Max-Wien-Platz 1, D-07743 Jena, Germany*
(Received 29 July 1994)

The $K\alpha_{1,2}$ and $K\beta_{1,3}$ spectra of copper were measured using double- and single-crystal diffractometers whose finite resolution effects were carefully characterized and corrected for. A phenomenological resolution of the spectra into Lorentzians is given, yielding excellent R factors close to 1%. Fits to our detailed relativistic Dirac-Fock and nonrelativistic Hartree-Fock *ab initio* calculations reveal that the line shapes can be accounted for by the diagram and the single $\underline{3d}$ spectator hole transitions only, with R factors of 3–5 % (the underline below $3d$ denotes a hole state). The contribution of the $\underline{3d}$ spectator transitions to each of the spectra is 26–30 %. The $K\alpha$ spectrum may also contain a small ~0.5% contribution from the $\underline{3p}$ spectator transition. The fit residuals of the $K\beta$ spectrum show systematic deviations in the vicinity of the β' feature, which may be due to exchange interactions or plasmon excitations. Contributions of similar origins to the $K\alpha$ spectrum were not detected. Linewidths, energies, and intensities are reported, for the raw as well as the fit-resolved spectra, and critically compared with previous data, where available.

PACS number(s): 32.30.Rj, 32.80.Hd, 31.30.Jv

I. INTRODUCTION

The structure of the x-ray diagram emission lines of the iron group transition elements has been the subject of numerous experimental and theoretical studies [1–6]. This was motivated by their asymmetric shapes, indicating large contributions from processes other than the main single electron bound-bound diagram transitions which dominate the corresponding symmetric emission lines of higher-z atoms. The large number of satellite lines, some of which have energies *lower* than those of the parent line and hence indicating a mechanism different from standard multielectronic excitation, has also motivated many of the studies [7–9]. Another motive, particularly important for the copper lines which are extensively used in a variety of x-ray diffraction experiments, is the need to obtain an accurate analytic representation for the line shapes. This is required for distinguishing features in the diffraction pattern originating in the sample from those due to the shape of the x-ray line. An example of such an application is given in Ref. [10].

The asymmetric line shape of the copper emission lines, the subject of the present study, was attributed to various different processes, namely the Kondo-like interaction of the conduction electrons with the core-hole states [11], final-state interactions between the core hole and the complete $3d$ shell [4], electrostatic exchange interaction of the $3d$ and $2p$ shells [5], and shake-up processes from the $3l$ shells [6, 12]. All these are multielectronic effects, going beyond the simple single-electron, frozen-atom description of the emission process. Thus they can yield, in principle, a better understanding of intrashell and intershell electronic correlations in atoms.

The $K\alpha_{1,2}$ line shapes were previously shown [13, 14] to be well described by the many-body conduction band excitation theory of Doniach and Šunjić [11], and, almost as well, by $3l$ shake-up processes [12]. Shake up from the $3d$ shell was also shown to account reasonably well for the measured $K\beta_{1,3}$ line shape, although a complete quantitative fit was not reported and possible contributions from other shells were not investigated [15, 16]. The low-energy satellite denoted $K\beta'$ received special attention, and several other sources such as exchange interaction [7, 9] and plasmon oscillations [8] were suggested as its origin. The agreement between theory and experiment on this feature is, however, only partial at best.

A prerequisite to an accurate measurement of the line shape is the determination of the various factors affecting the resolution of the measuring system, and their relative importance. We have recently completed such a study [17], which resulted in a high accuracy characterization of the system used in the present measurements. This study allowed the minimization of distortions due to finite resolution in the measurements presented here. Additional advantages of the present study over previous ones are the few-ppm ($K\beta$) or less ($K\alpha$) level of accuracy in the absolute energy scale and the fact that both the α and β spectra were measured using the same well characterized experimental setup under well defined resolution conditions. Finally, we have carried out relativistic and nonrelativistic atomic calculations to elucidate the internal structure of the lines. These assumed that the line shape can be fully accounted for by satellites resulting from $\underline{3l}$ spectator holes in addition to the nominal single electron diagram transitions (underlining indicates hole

states throughout this paper). We have found that such a description can indeed account extremely well for the $K\alpha$, and to a somewhat lesser extent, also the $K\beta$ spectra. The experimental and calculational details are presented in the next two sections, with the third section presenting and discussing the results. The fourth section details our conclusions and suggestions for future work.

II. EXPERIMENT

The measured spectral distribution of an emission line differs, in general, from the true distribution due to the modifications introduced by the instrumental function of the spectrometer (spectrometer window function). To obtain the true distribution, either the instrumental function must be much narrower than the spectral distribution, or it must be separated out somehow from the measured intensity distribution [18]. The experimental parameters should be, therefore, chosen in a way that minimizes these distortions, and consequently also the required corrections. In Ref. [17] we presented the solution of this problem for single- and double-crystal spectrometers. We took into account the influences of collimator geometry, crystal reflection curves according to dynamical theory including the variation of their shape with the wavelength, tube arrangement, absorption of the radiation in the anode, air, and windows. It was possible to simulate the influence of various experimental parameters, to conclude under which conditions a convolution of the true spectral distribution and the (approximated) instrumental function is a good approximation for the measured intensity distribution, and under what conditions the instrumental function was negligible. On this basis optimized parameters were chosen to carry out the measurements reported here.

Single- (SC) and double-crystal (DC) diffractometric measurements were carried out. The single-crystal spectrometer (classical Bragg configuration [19]) allowed for the measurement of absolute angles with high precision and accuracy. The mean total angle dividing error is 0.12 arcsec and the smallest angular step is 0.06 arcsec [20]. This device has been used mainly for the determination of absolute lattice parameters according to the Bond method [21]. It allows the determination of the lattice parameter of silicon, using the (444) reflection and Cu $K\alpha_1$ radiation, with a reproducibility (precision) of about 3×10^{-8} nm and an accuracy of 1.5×10^{-7} nm [22]. Using a calibrated silicon crystal an absolute wavelength determination in nm is possible [22]. The conversion factor to the energy scale is 8.065 541 0 $\times10^5$ $(\mathrm{m\,eV})^{-1}$ which carries an uncertainty of 3×10^{-7} [23].

The following experimental parameters were used: symmetrical silicon (444) reflection for the Cu $K\alpha$ spectrum, asymmetrical (553) reflection for the Cu $K\beta$ spectrum, tube nearly perpendicular to the diffraction plane, tube voltage and current of 40 kV and 30 mA, respectively, collimator length of 390 mm, (horizontal), slit widths of 0.03 mm for the Cu $K\alpha$ radiation, and 0.10 mm for the Cu $K\beta$ radiation, and a (vertical) slit height of 0.42 mm. Under these conditions the measured intensity distribution is well approximated by a convolution of true spectral distribution and the (approximated) instrumental function. The true distribution was obtained in this case by deconvolution of the measured spectrum. The analytic relation between the exact instrumental function and the spectral distribution was used only to confirm that the window function approximation employed was indeed valid.

The double-crystal spectrometer measurements were carried out with the commercial DTS spectrometer [24]. An advantage of the double-crystal arrangement is that the angular scale is stretched by a factor of 2. Thus a better angular resolution can be obtained as compared with the single-crystal mode of the same spectrometer. However, since the zero angle of this device could not be determined accurately, the corresponding energy scale is relative only. The angular position of the maximum of the Cu $K\alpha_1$ peak was defined to be $\lambda_0 = 0.154\,059\,292$ nm [22]. For the double-crystal spectrometer it was possible to make the instrumental function very narrow, so that no correction for window function effects was necessary. Fits were done with the measured and smoothed data, applying only a correction for absorption [17].

The following experimental parameters were used: symmetric silicon (333) reflections in both crystals for all spectra. The (444) reflection was out of the range of the spectrometer. The tube was nearly perpendicular to the diffraction plane, tube voltage, and current of 40 kV and 45 mA, respectively, collimator length of 560 mm, (horizontal) slit widths of 1.0 mm (focus side) and 10 mm (sample side) for both spectra, and (vertical) slit heights of 0.4 mm for the Cu $K\alpha$ radiation and 0.8 mm for the Cu $K\beta$ radiation.

III. ATOMIC STRUCTURE CALCULATIONS

A. Introduction

We have considered transitions involving up to two-vacancy states, of the forms $\underline{1s}\rightarrow\underline{np}$ and $\underline{1s3l}\rightarrow\underline{np3l}$ where $n = 2,3$ for $K\alpha$ and $K\beta$, respectively, and $\underline{l} = s,p,$ or d. The first set of transitions are the so called diagram lines while the second are the $\underline{3l}$-spectator vacancy satellites. The calculations were done using both the relativistic Dirac-Fock (DF) code GRASP of Grant and co-workers [25] and the nonrelativistic Hartree-Fock (HF) code HF86 of Froese Fischer [26], both supplemented by programs written in house, as detailed below.

B. Energy calculations

Previous studies [27,28] indicate the importance of taking into account rearrangement and full relaxation of the atom prior to the emission process. To do so, we have generated in all cases the initial and final state wave functions in separate single configuration runs where the wave functions and energies of *all* orbitals were allowed to vary.

The input to both programs is specified by the electronic occupation numbers of each shell in nonrelativistic notation. Although the HF code employs the LS coupling notation while the DF one uses jj coupling, the end

results for both calculations are intermediate coupling ones. In practice, considerable mixing of states results in all of the two-hole calculations. The DF code, which was used in the average level (AL) optimization mode, takes into account all possible couplings between the electrons in open shells. It calculates and lists the fully split energy level scheme for the given configuration. By contrast, the HF code provides only the average energy of the configuration, as well as values of the various Slater integrals and the spin-orbit parameters. These were used to set up the intermediate coupling Hamiltonian matrix including the spin-orbit terms, following Condon and Shortley [29] and Slater [30]. The Hamiltonian was diagonalized to yield the energy levels of the multiplet. Note that following common practice [28], the calculated spin-orbit parameters were scaled by the ratio of the calculated-to-measured spin-orbit splitting of the diagram lines [28]. Also, since relativistic effects are considerable for the $1s$ level, nonrelativistic HF values involving this level are known to be greatly in error. This was corrected for by shifting the average energy of all the relevant multiplets by the energy difference between the calculated and measured average energy of the $K\alpha$ diagram lines [28]. As in previous studies [15, 12–14] the $4s$ electron of the Cu atom was neglected in all calculations. Thus, the only open shells are those of the active electrons. The number of levels in the HF approximation in this case is equal, therefore, to that of the fully split DF levels, and so is, of course, the number of lines. Finally, the transition energies for the various lines were calculated by taking the difference in energy of pairs of levels from separate runs, as allowed by electric dipole selection rules.

C. Line strength calculations

Although GRASP provides a means for calculating the relative transition probabilities within a multiplet, this can only be done when the wave functions of the initial and final states are orthogonal, which is clearly not the case here, since the initial and final states were generated in separate runs. We have used, therefore, configuration interaction calculations to obtain the various transition probabilities using once the frozen orbitals of the initial state and again those of the final state. The two values were within ~10% of one another for all lines stronger than ~5% of the strongest line. Thus in the fits and figures presented here we have used line strengths calculated from the initial state wave functions. This amounts to using the frozen-atom approximation to calculate the line strengths within each multiplet. We have verified that the use of final state wave functions has a marginal effect on the results as presented here and no influence on our final conclusions.

In the absence of an appropriate code, the line strengths for the HF calculations were approximated by those of the pure LS coupled atom, which are given, for example, by Cowan [31]. Although the intermediate coupling results in a considerable mixing of the pure LS states, previous studies by Scott and co-workers [28] on the satellite lines of the iron group elements indicate that this approximation is reasonable for the strongest lines. A comparison of the pure LS line strengths to those obtained in our relativistic DF results also supports this conclusion, as shown in the next section.

IV. RESULTS AND DISCUSSION

A. The $K\alpha$ spectrum

1. *Analytic representation*

The $K\alpha$ spectrum, measured in the DC configuration, is shown in Fig. 1. As a sensitive measure for the quality of our data, Table I lists the full width at half maximum of the $K\alpha$ lines, along with earlier results. Note the good agreement with the previous measurements for $K\alpha_1$, and the twofold higher accuracy of our measurements. The biggest deviation, that of Ayers and Ladell [33], is still less than twice the combined standard deviation. The agreement among the $K\alpha_2$ values is less good, although still reasonable except for that of Citrin *et al.* [32] which was already commented on by Ayers and Ladell [33] and Sørum [3]. As finite resolution effects are significant in these measurements [33, 17, 34], we included in Table I only values corrected for these effects. Other studies (see Refs. [13, 14, 17, 35] for a discussion.), where corrections for these effects were not applied, yield values larger by 0.2–0.4 eV.

The resolution corrected spectrum was fitted by four

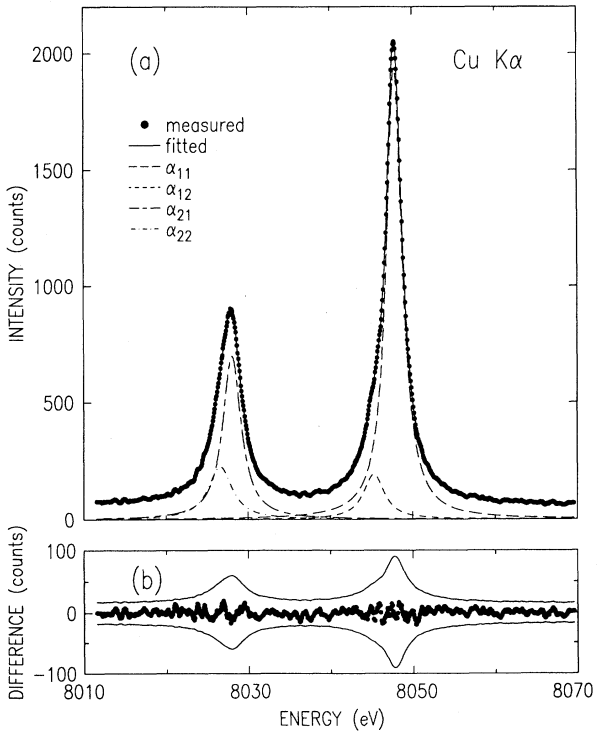

FIG. 1. (a) Double-crystal spectrometer measured Cu $K\alpha_{1,2}$ spectrum and fitted Lorentzians. The fit parameters are given in Table II. (b) Lorentzian fit residuals. The thin lines denote the $\pm 2\sigma$ values of the data, where σ is the standard deviation.

TABLE I. Widths of the raw Cu $K\alpha$ spectrum, corrected for resolution effects. Error estimates in the last digits are given in parentheses, where available.

	Cu $K\alpha_1$ (eV)	Cu $K\alpha_2$ (eV)
Bearden and Shaw[a](1935)	2.47	3.31
Pessa[b](1973)	2.30	3.14
Citrin *et al.*[c](1974)	2.39(10)	2.89(10)
Berger[d](1986)	2.37	3.35
Sørum[e](1987)	2.28(5)	2.78(5)
Ayers and Ladell[f](1988)	2.41(5)	3.17(21)
This work	2.29(2)	3.34(6)

[a] Reference [40].
[b] Reference [53].
[c] Reference [32].
[d] Reference [39].
[e] Reference [3].
[f] Reference [33].

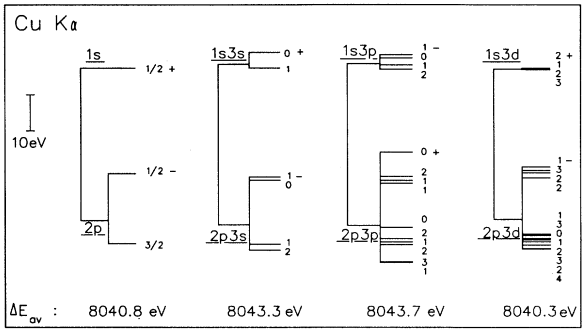

FIG. 2. DF-calculated energy level diagram for the one-hole and two-hole initial and final states of the $K\alpha$ transitions. Level splitting in each state, but not that between upper and lower states, is drawn to scale. The difference in the average energy of the upper and lower states is given below each pair. Due to the considerable mixing the levels are denoted as J^p only, where J is the total angular momentum and p is the parity.

Lorentzians, and the results are shown in Fig. 1. Each Lorentzian is defined by its position E_{ij}, width W_{ij}, and relative intensity I_{ij}, where $i = 1, 2$ denotes $K\alpha_{1,2}$, respectively, and j is the index within each line. The fit parameter values are given in Table II. As can be seen from the small and nonsystematic residuals in Fig. 1 the fit is very good, and an R factor of 1.4% is achieved. The fit and the resulting parameter values were discussed and compared with earlier measurements in Ref. [17] and will not be discussed here further.

2. *Comparison with theory*

In the atomic structure calculations, we considered in addition to the diagram transitions $\underline{1s}\rightarrow\underline{2p}$ also the two-hole transitions $\underline{1s3l}\rightarrow\underline{2p3l}$ where $l = s, p, d$, and the most probable three-hole transition $\underline{1s3d^2}\rightarrow\underline{2p3d^2}$. The relativistically calculated energy level scheme for the one- and two-hole states is shown in Fig. 2. Since the intermediate coupling results in a considerable mixing of the pure LS, or jj, states, the levels can only be labeled as J^p , where J is the total momentum and $p = \pm$ is the parity. These are given in the figure. ΔE_{av} denotes the difference in the $(2J + 1)$-averaged energy of the upper and lower states.

The DF "stick diagrams" of the transitions for the various multiplets are given in Fig. 3, and the corresponding figure for the nonrelativistic HF calculations is shown in Fig. 4. Although the details of the line positions and, in particular, the intensities are different in the two calculations for reasons discussed in the previous section, the overall spectral shape is similar for a given multiplet in both calculations. The lifetime widths of the transitions, which are larger than the interline distances, result in a smooth line shape of overlapping contributions and it is not possible to identify by eye the individual contributions of the various multiplets. Thus only general conclusions can be drawn from eye inspection. For example, the strongest lines of the $\underline{1s3p}\rightarrow\underline{2p3p}$ multiplet are in a region where the measured intensity is small, and hence the contribution of this multiplet to the line shape cannot be large.

3. *Theoretical fits*

To obtain a more quantitative assessment of the contributions of the various multiplets to the line shape , we

TABLE II. Lorentzian fit parameters for the Cu $K\alpha_{1,2}$ lines measured using a single- and double-crystal spectrometer. The lines are fitted by four symmetric Lorentzians, whose positions, widths, and intensities (normalized to the measured maximum of the $K\alpha_1$ line) are listed. Note the excellent R factors of the fit.

Line	Double crystal			Single crystal		
	Energy (eV)	Width (eV)	Intensity (Rel.)	Energy (eV)	Width (eV)	Intensity (Rel.)
α_{11}	8047.837(6)	2.298(7)	0.942(6)	8047.837(2)	2.285(3)	0.957(2)
α_{12}	8045.293(52)	3.068(64)	0.094(3)	8045.367(22)	3.358(27)	0.090(1)
α_{21}	8028.022(13)	2.710(17)	0.339(4)	8027.993(5)	2.666(7)	0.334(1)
α_{22}	8026.562(40)	3.560(57)	0.110(3)	8026.504(14)	3.571(23)	0.111(1)
R factor(%)		1.3			0.69	

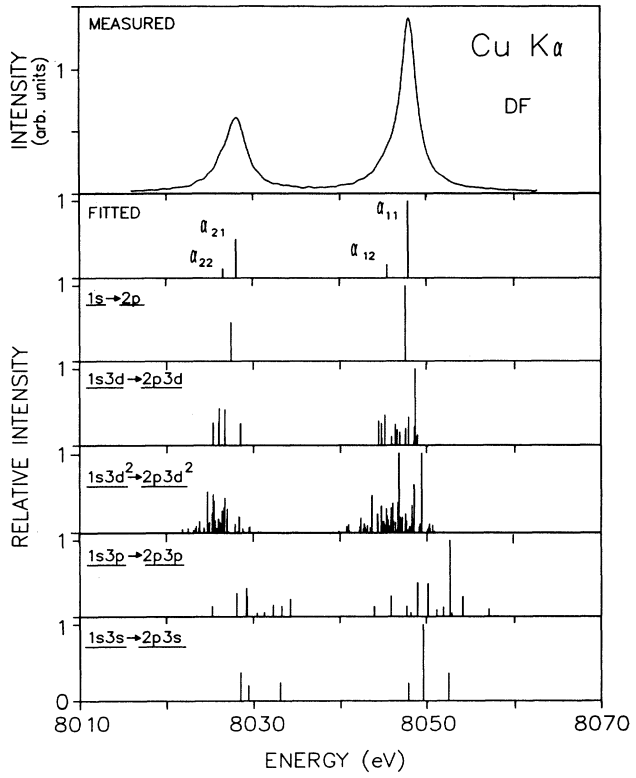

FIG. 3. Measured, Lorentzian-fitted, and DF-calculated transitions for the $K\alpha$ spectrum. Calculated intensities in each multiplet are relative to the strongest line of that multiplet.

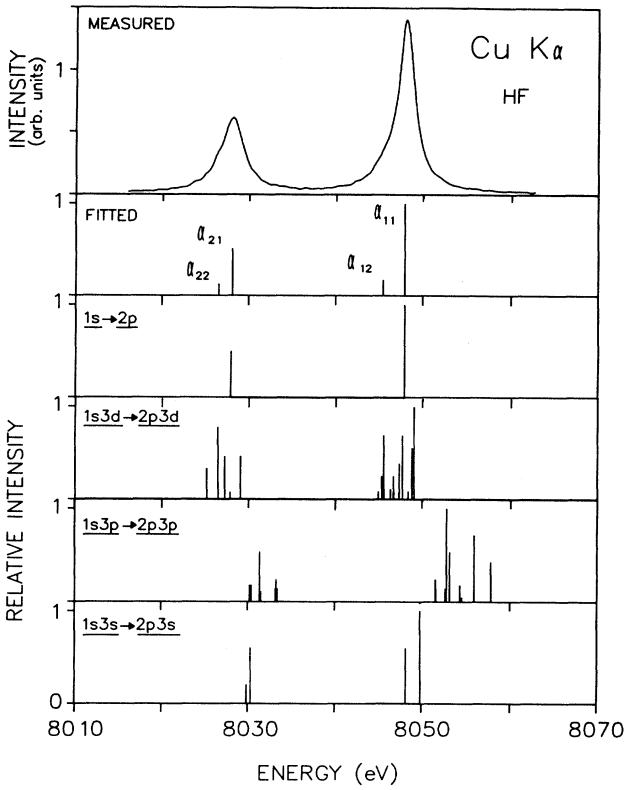

FIG. 4. Same as Fig. 3 but for HF calculated transitions.

have carried out detailed model fits to the data, using the DF calculated line strengths and energies as inputs. Each calculated line was represented by a Lorentzian within the following model:

$$I_c(E) = c_0 + d_0 E + \sum_{m=1}^{M} a_m \sum_{l=1}^{L} b_{lm} / \{1 + [(E - E_{lm} - s_m)/w_m]^2\}, \quad (1)$$

where c_0, d_0 define a linear background and $\sum_{m,l}$ sum over the different multiplets (m) and the lines within each multiplet (l). a_m, s_m, and w_m are the amplitude, energy shift relative to the calculated position and the width, all of which are common to all the lines of a multiplet. Finally, E_{lm}, b_{lm} are the energy positions and calculated intensities of each line within the multiplet, which are fixed at the values obtained in the calculations and do not vary in the fit. For each multiplet included in the fit the three corresponding parameters, a, s, w, can be allowed to vary in the fit. In addition, c_0, d_0 are also varied. Since the DF calculations are accurate to no better than 1–2 eV [28, 25] we have allowed separate shifts $s_{1,2}$ and separate widths $w_{1,2}$ for the two diagram lines. To minimize the number of free parameters in the fit, for each multiplet a single width, common to all lines, was used. Also, a single shift s_3, common to all multiplets, was employed.

A series of fits with different combinations of the diagram lines with one or more multihole multiplets were carried out, for both the DC and SC data. The results obtained in some of the cases are given in Table III. It can be seen clearly that the fits involving the diagram transition (a), or the diagram transitions plus a $\underline{3s}$ or $\underline{3p}$ spectator (b) and (c) are inferior to those including the $\underline{3d}$ spectator (d) and (g). Furthermore, the inclusion of either $\underline{3s}$ or $\underline{3p}$, or both, in addition to the $\underline{3d}$ hole does not improve the fit. The inclusion of the two-hole spectator (g) makes only a marginal improvement in the goodness of fit (GoF), while its intensity is driven to zero. Note also that the fits are robust, i.e., the values of the various parameters obtained in fits (a) and (d) remain unchanged upon the inclusion of the $\underline{3s}$ and $\underline{3p}$ transitions, fits (b) and (c) and (e)–(g), respectively. The best fit to the DC data, (d), is shown in Fig. 5, along with the residuals. Note that all residuals are within 2σ, and are randomly distributed. This, and the GoF< 1, indicate that the model exhausts the accuracy of the data.

These results lead to a clear conclusion that the only appreciable contribution to the lines besides the diagram transitions is from the $\underline{3d}$ spectator hole transition, in agreement with earlier results [12, 5] based on nonrelativistic HF calculations.

4. Intensities and line widths

The fits allow one to separate out the individual contributions of the one- and two-hole processes to the line

TABLE III. Fit results for the DC-measured $K\alpha_{1,2}$ spectrum. The following fits are listed: (a) $1s\rightarrow 2p$ transitions only; (b) $1s\rightarrow 2p+1s3s\rightarrow 2p3s$; (c) $1s\rightarrow 2p+1s3p\rightarrow 2p3p$; (d) $1s\rightarrow 2p+1s3d\rightarrow 2p3d$; (e) $1s\rightarrow 2p+1s3d\rightarrow 2p3d+1s3p\rightarrow 2p3p$; (f) $1s\rightarrow 2p$ plus all three multiplets; (g) $1s\rightarrow 2p+1s3d\rightarrow 2p3d+1s3d^2\rightarrow 2p3d^2$. The values listed are the fit result. No constraint on intensities was employed. I_{int} is the integrated intensity relative to that of the full spectrum. Units are given in parentheses.

Parameter		(a)	(b)	(c)	(d)	(e)	(f)	(g)
Shift $2p_{3/2}$(eV)	s_1	0.31	0.31	0.31	0.28	0.28	0.28	0.27
$2p_{1/2}$	s_2	0.39	0.39	0.39	0.55	0.55	0.55	0.55
$2p3l$	s_3	0.00	2.00	1.53	0.02	0.02	0.02	0.02
Width $2p_{3/2}$(eV)	w_1	2.62	2.62	2.62	2.09	2.08	2.07	2.06
$2p_{1/2}$	w_2	3.31	3.31	3.31	2.69	2.68	2.67	2.66
$2p3s$	w_3		2.21				12.04	
$2p3p$	w_4			2.69		5.56	9.94	
$2p3d$	w_5				2.75	2.71	2.68	2.28
$2p3d^2$	w_6							8.00
Intensity $2p_{3/2}$ (Rel.)	a_1	1.000	1.000	1.001	0.852	0.862	0.862	0.861
$2p_{1/2}$	a_2	0.431	0.431	0.431	0.350	0.357	0.357	0.357
$2p3s$	a_3		0.0				0.001	
$2p3p$	a_4			0.0		0.001	0.0	
$2p3d$	a_5				0.063	0.066	0.067	0.067
$2p3d^2$	a_6							0.002
Background (Rel.)	c_0	0.036	0.036	0.036	0.038	0.038	0.037	0.037
Background (10^{-5}/eV)	d_0	3.11	3.11	1.56	5.18	3.11	2.59	3.11
I_{int} $2p_{3/2}$ (%)		64.7	64.7	64.8	45.8	45.0	44.8	44.1
$2p_{1/2}$		35.3	35.3	35.2	24.2	24.1	23.9	23.5
$2p3s$			0.0				0.7	
$2p3p$				0.0		0.5	0.4	
$2p3d$					30.0	30.4	30.2	25.4
$2p3d^2$								7.0
R factor (%)	R_w	7.0	7.0	7.0	3.0	3.0	3.0	3.0
Goodness of fit	GoF	1.14	1.15	1.15	0.51	0.51	0.51	0.49

shapes. The linewidths and relative intensities of the one- and two-hole lines contributing to the spectrum are compared in Table IV with the other experimental, semiempirical, and *ab initio* calculations. As can be seen, our $K\alpha_1$ widths are in good agreement with the experimental and theoretical values. Sauder's value [12], obtained by fits to his measured x-ray emission spectrum, is lower by $\sim$10% than both experimental and all of the theoretical values. The excellent agreement of our one-hole width with the calculated *lifetime* widths further supports our conclusion that only two processes contribute to the measured x-ray line shape; the diagram and the $3d$-spectator transitions. It also supports an earlier suggestion by Fuggle and Alvarado [36] concerning the discrepancy between their XPS-measured and the calculated L_3 level width, where the discrepancy was assigned to level broadening due to multiplet splitting involving the $3d$ electrons.

The scatter in the $K\alpha_2$ values in Table IV is consider-

TABLE IV. Linewidth (W) and integrated intensities (I) for the one- and two-hole components of the $K\alpha$ spectrum. Present values are taken from fit (e) of Table III to allow better comparison with the results of Sauder *et al.* [12]. The intensities of the single-electron spectrum was taken as 100%.

		Experiment			Theory			
		Present	Sauder[a]	Yin[b]	Krause[c]	Chen[d]	Yin[e]	CC[f]
W	$2p_{3/2}$ (eV)	2.08	1.81(5)	2.09(11)	2.11(15)	2.14	2.07	2.05
	$2p_{1/2}$	2.68	2.93(7)	2.53(12)	2.17(15)	2.15	2.96	2.04
	$2p_{3/2}3d$	2.75 [g]	1.21(15)					
	$2p_{1/2}3d$	2.75 [g]	1.09(15)					
I	$2p3d$ (%)	44	38.(3)					
	$2p3p$	0.7	3.0					

[a] Fit to x-ray emission spectrum. Reference [12].
[b] XPS-measured L width from Ref. [37] and semiempirical K-level width from Ref. [54].
[c] Semiempirical. Reference [54].
[d] K-level width taken from Ref. [38] and L-level widths taken from Ref. [55].
[e] K-level width taken from Ref. [38] and L-level widths taken from Ref. [37].
[f] K-level width of 1.44 eV and L-level widths of 0.599 and 0.613 eV for L_2 and L_3, respectively, from Ref. [51].
[g] A single width was used for all lines of the $3d$ spectator transition.

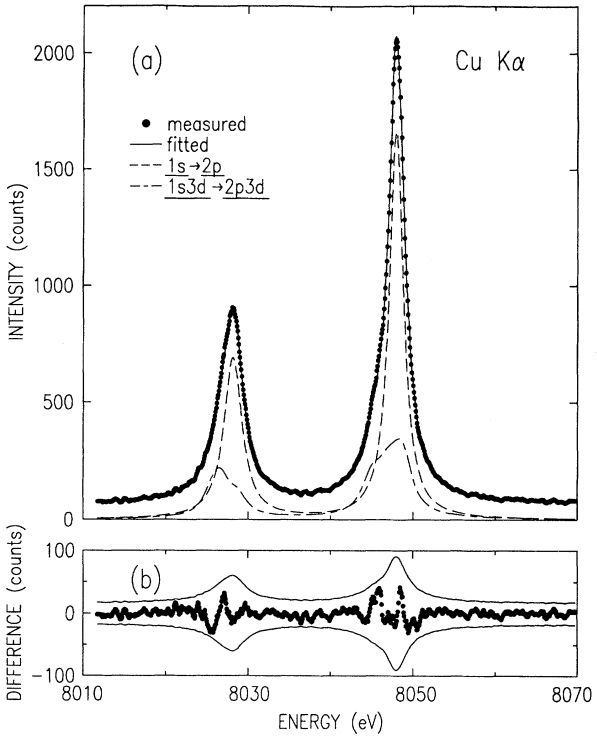

FIG. 5. (a) Double-crystal measured $K\alpha_{1,2}$ spectrum and best fit to the DF-calculated transitions indicated. The fit parameters are given in column (e) in Table III. (b) Fit residuals. The thin lines denote the $\pm 2\sigma$ values of the data. Note the excellent fit indicated by the small, and randomly distributed, residuals.

ably larger than for $K\alpha_1$. Here the experimental results are within ~14%, while three of the theoretical values underestimate it by more than 30%. The reason for the discrepancy can be traced to the calculated L_2 level width. The theoretical calculations, which considered only isolated atoms, neglected the extra broadening due to the L_2-$L_3M_{4,5}$ Coster-Kronig decay. While these processes are energetically forbidden in many isolated atoms [36], it is significant for solid Cu anodes used in x-ray emission measurements. As shown by Yin *et al.* [37] and Fuggle and Alvarado [36], its inclusion yields L-level widths in good agreement with XPS measurements. Using these L-level widths, along with the Dirac-Hartree-Slater (DHS) K-level widths of Chen *et al.* [38] yield the values listed under Yin in Table IV. Including only the L_2-L_3M_5, but not the L_2-L_3M_4, reduces the width to 2.36 eV [37], still in better agreement with the measurements than the free-atom calculations. The good agreement of our and Yin *et al.*'s measured values for $K\alpha_2$ with each other and with the theoretical results, supports, again, our conclusion for the origins of the line shape.

In contrast with the reasonable agreement observed for the widths of the diagram lines, there is a considerable discrepancy between the two-hole linewidths obtained by Sauder *et al.* and us. It is highly unlikely that the additional $3d$ hole would extend the lifetimes of the $1s$ and $2p$ levels so that the corresponding widths would be reduced to about one-half ($K\alpha_1$) or one-third ($K\alpha_2$) of the single hole width. Rather, it is conceivable that the sharp features observed by Sauder *et al.*, but not confirmed in several subsequent independent studies [13, 14, 39, 3, 17], forced narrower widths for the two-hole lines in the fitting routine.

Both Sauder's and the present study agree, however, on the large, ~40%, and small, 1–3 %, contributions of the $3d$ and $3p$ spectator transitions, respectively, to the x-ray emission process. A theoretical prediction for these values, which, to the best of our knowledge, is not available in the literature, would be most desirable for elucidating the details of the emission process.

B. The $K\beta$ spectrum

1. Analytic representation

The DC-measured and resolution-corrected $K\beta$ spectrum is shown in Fig. 6. As noted earlier [40] four underlying lines are discernible. These were denoted as the two diagram lines β_1 and β_3 and two satellites; β' on the low-energy side, and β'' on the high-energy side. A fifth line was proposed by Bremer and Sørum [16], but no determination of its position, intensity, and width was carried out. Hayasi [41] also observed this feature and determined its energy without a detailed fit. Bremer and Sørum also observe a very sharp dip just off the peak,

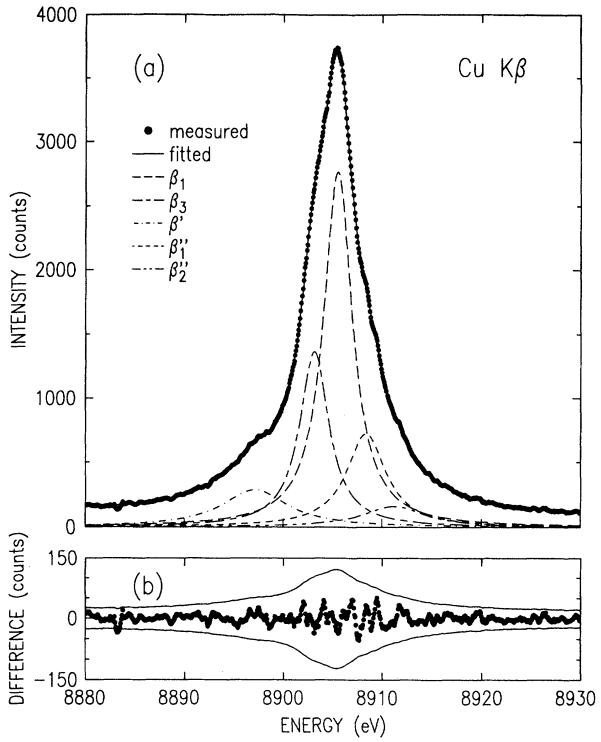

FIG. 6. Same as Fig. 1 but for the $K\beta_{1,3}$ spectrum. Fit parameters are given in Table V.

TABLE V. Lorentzian fit parameters for the DC-measured Cu $K\beta_{1,3}$ spectrum. Previous estimates of the energies of the various features are also given. E, W, and I are the energy, full width at half maximum, and intensity relative to the measured $K\beta_{1,3}$ maximum, respectively.

Line	Parameter	Four Lorentzian	Five Lorentzian	Bearden and Shaw[a]	Cauchois and Senemaud[b]
β_1	E (eV)	8905.489(8)	8905.510(8)	8905.29	8905.14
	W (eV)	3.72(1)	3.64(1)		
	I (Rel.)	0.720(3)	0.741(3)		
β_3	E	8903.098(16)	8903.119(15)	8902.9	8902.8
	W	3.43(2)	3.53(2)		
	I	0.321(3)	0.345(3)		
β'	E	8897.057(62)	8897.117(60)	8896.3	8897.4
	W	7.62(11)	7.87(10)		
	I	0.070(1)	0.074(1)		
β_1''	E	8908.449(30)	8908.488(30)		8909.3
	W	6.63(4)	4.63(4)		
	I	0.209(2)	0.180(2)		
β_2''	E		8911.15(13)	8911.7	8913.0
	W		7.41(20)		
	I		0.040(1)		
R factor (%)		1.12	1.01		

[a] References [40, 56].
[b] Reference [41].

on the low-energy side, where only a smooth shoulder was observed in earlier measurements. This was assigned to the spin-orbit splitting of the two diagram lines. No such dip was observed in any of the other published line shapes, nor in our measurements. Finally, although the position of the $K\beta'$ feature as measured by Salem *et al.* [9] is in good agreement with theory, its intensity disagrees with both the exchange interaction [9, 7] and plasmon oscillation [8] theories.

To address these issues, a series of fits of the spectrum with an increasing number of Lorentzians was carried out. The fits indicate that although a reasonable fit can be obtained by using four Lorentzians only, a fifth one is required on the high-energy side of the spectrum to obtain the best fit. The results of the four- and five-Lorentzians fits are summarized in Table V. The reduction in the R factor upon inclusion of the fifth Lorentzian is significant. Our fit-resolved lines agree well with the previous, unresolved, measurements, even for the weak $K\beta_2''$ line. They also provide estimates for the relative intensities of these lines, not previously available. Finally, it should be noted that the four-Lorentzian fit yields the single β'' line at the position of the lower-energy component β_1'' rather than at the higher-energy component β_2'', which was denote as β'' in Bearden's four-line description of the spectrum.

The 2.39(2) eV obtained here for the β_1-β_3 line separations is in close agreement with other values obtained for this quantity, as shown in Table VI. The best agreement is with the 2.4 eV XPS measurement of Cuthill and Erickson [42], the 2.5 eV relativistic calculations of Huang

TABLE VI. The energy splitting Δ of the $3p_{1/2}$ and $3p_{3/2}$ levels in Cu.

Source	Δ (eV)
Experimental	
Bearden[a] (1935)	2.0
McAlister[b] (1975)	2.0
Cuthill[c] (1975)	2.4
Madden[d] (1978)	2.7
Bruhn[e] (1979)	2.25
LaVilla[f] (1979)	2.4
Bremer[g] (1979)	2.2
Fuggle[h] (1980)	2.2
Present	2.39
Theoretical	
Herman[i] (1963)	2.7
Huang[j] (1976)	2.55
Misra[k] (1992)	2.49
Present DF	2.55

[a] Reference [40]. Unfolding of x-ray emission data.
[b] Reference [46]. Soft x-ray emission.
[c] Reference [42]. X-ray photoemission.
[d] Reference [45]. Auger spectroscopy.
[e] Reference [57]. Soft x-ray photoabsorption in vapor.
[f] Reference [15]. X-ray emission.
[g] Reference [16]. X-ray emission.
[h] Reference [58]. Electron spectroscopy.
[i] Reference [59]. Analytic nonrelativistic Hartree-Fock.
[j] Reference [43]. Relativistic Dirac-Hartree-Fock-Slater.
[k] Reference [44]. Modified Moseley plot.

et al. [43] and us, and the recent 2.5 eV Moseley plot determination of Misra *et al.* [44]. The worst agreement is with the 2.7 eV Auger measurements of Madden *et al.* [45] and the 2.0 eV deconvoluted x-ray emission results of Bearden and Shaw [40] and McAlister *et al.* [46]. While a clear cut conclusion can not be made on the basis of this data, a value close to 2.5 eV seems to be the most widely accepted. Theoretical assignments for the various features listed in Table V are discussed in the next two subsections.

2. *Comparison with free-atom theory*

As shown by the nonrelativistic HF calculation of LaVilla [15], the β' and β'' satellites coincide rather well with the $\underline{3d}$ spectator hole transition lines, the only two-hole transitions considered in that study. As for $K\alpha$, we considered the diagram transitions $\underline{1s}\rightarrow\underline{3p}$, the single spectator hole transitions $\underline{1s3l}\rightarrow\underline{3p3l}$ where $l = s, p, d$, and the most probable two-spectator-hole transition $\underline{1s3d^2}\rightarrow\underline{3p3d^2}$. The calculated realtivistic DF energy level scheme for the diagram and one-spectator hole states is shown in Fig. 7 . The DF levels can be labeled, again, as J^p only, due to the strong mixing.

The DF and HF transition multiplets are shown in Figs. 8 and 9, respectively. As in the case of $K\alpha$, the two calculations show an overall similarity, although the details of the line positions and, in particular, the intensities are different. The overlap here is, however, even greater than for $K\alpha$, as even the diagram line separation is only ~2.5 eV. While the separation of these lines is obtained correctly in the DF calculations, their average energy is downshifted by 2.6eV. Similar unexplained few eV shifts in the calculated average energy of multiplets were observed by others as well [28, 47], and, when identified and taken care of, are of little consequence.

A visual inspection of Fig. 8 reveals that the $\underline{3d}$ spectator hole multiplet has strong lines in the vicinity of the β', β_1'' and β_2'' features, as observed by LaVilla. The $\underline{3p}$ and $\underline{3s}$ spectator transitions are, however, also well aligned with the high energy satellites, and a small contribution to these features from the three-hole $\underline{3d^2}$ transitions can not be ruled out.

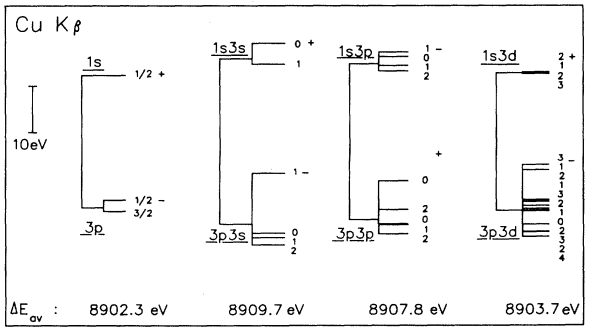

FIG. 7. Same as Fig. 2 but for the $K\beta$ transitions.

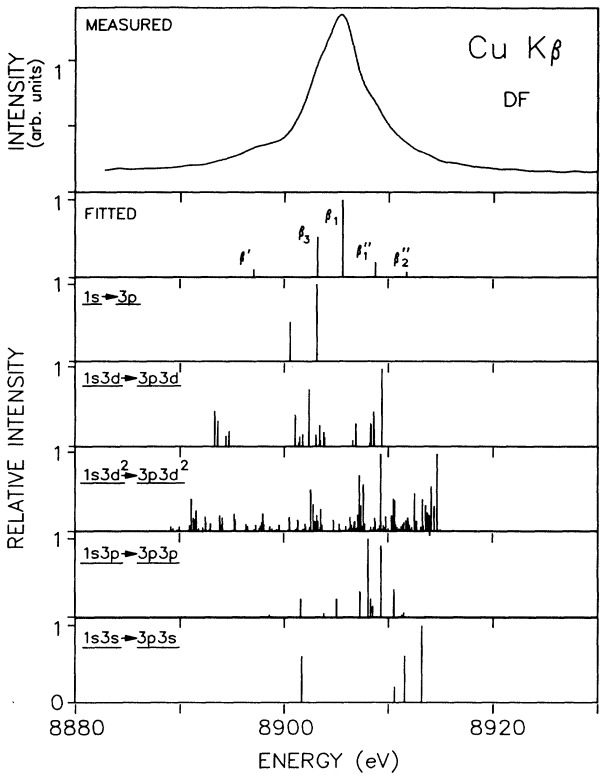

FIG. 8. Same as Fig. 3 but for the $K\beta_{1,3}$ spectrum.

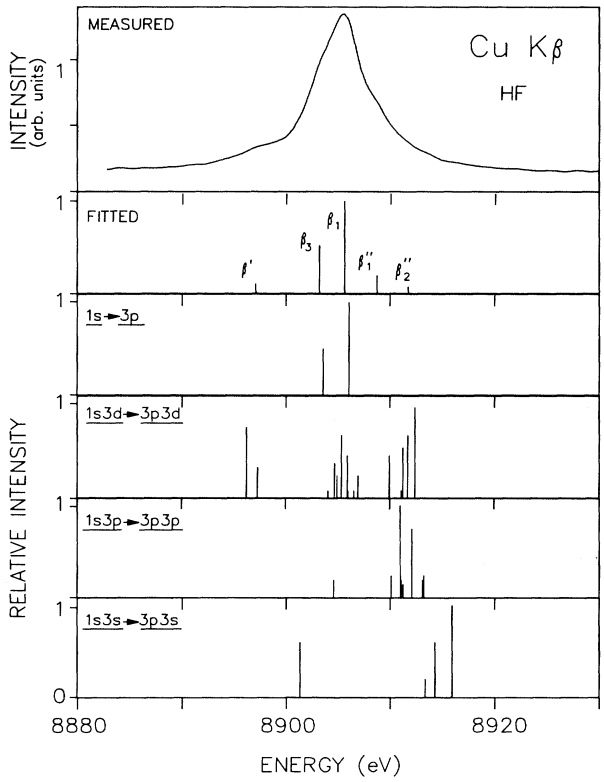

FIG. 9. Same as Fig. 4 but for the $K\beta_{1,3}$ spectrum.

3. Free-atom theoretical fits

As for $K\alpha$, we have carried out a series of fits to the measured data with various combinations of the calculated diagram and spectator spectra. The model is similar to that of the $K\alpha$ fits. However, since the overlap of the lines here is much greater, additional constraints had to be imposed to obtain convergence. We have therefore required that $I_{int}(K\beta_3)/I_{int}(K\beta_1) = 0.51$, where I_{int} is the integrated intensity. This ratio is predicted theoretically [48], and is in excellent agreement with previous experimental results (see Ref. [15]). We have also checked that the same constraint, when imposed on the $K\alpha$ fits results in a negligible change from the results cited above for the unconstrained fit. In addition, we constrained the two diagram lines to have the same shift s_1, since no evidence is available to the contrary, and since the small total width of the measured spectrum (~6 eV, as compared to ~23 eV for $K\alpha$) does not allow much latitude anyway.

The parameters obtained in the various fits are given in Table VII. As can be seen, the addition of a single $\underline{3s}$ or $\underline{3p}$ spectator spectrum to the diagram lines in (b) and (c) results in unphysical line widths of tens of eV's. The addition of a $\underline{3d}$ spectator spectrum, however, in (d) results in a pronounced reduction in the GoF and R_w values without producing any unphysical parameter values. Adding both $\underline{3p}$ and $\underline{3d}$ spectator spectra results in a further (small) reduction in the fit criteria, although the resultant $\underline{3p}$ width, 14.4 eV wide, is unphysical. Finally, adding the $\underline{3d^2}$ spectator spectrum while improving the fit yields an unphysical 49 eV width for the lines. We can conclude therefore that the fits indicate that in addition

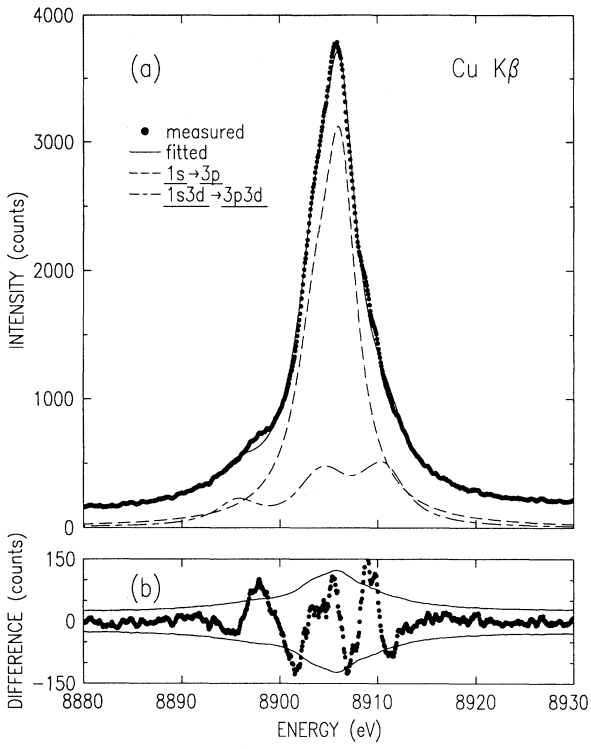

FIG. 10. Same as Fig. 5 but for the $K\beta_{1,3}$ spectrum. The fit parameters are given in column (d) in Table VII. Note the systematic deviations in the residuals. For a discussion of their possible sources see text.

TABLE VII. Fit results for the DC-measured $K\beta_{1,3}$ spectrum. The following fits are listed: (a) $\underline{1s}\rightarrow\underline{3p}$ transitions only; (b) $\underline{1s}\rightarrow\underline{3p}+\underline{1s3s}\rightarrow\underline{3p3s}$; (c) $\underline{1s}\rightarrow\underline{3p}+\underline{1s3p}\rightarrow\underline{3p3p}$; (d) $\underline{1s}\rightarrow\underline{3p}+\underline{1s3d}\rightarrow\underline{3p3d}$; (e) $\underline{1s}\rightarrow\underline{3p}+\underline{1s3d}\rightarrow\underline{3p3d}+\underline{1s3p}\rightarrow\underline{3p3p}$; (f) $\underline{1s}\rightarrow\underline{3p}+\underline{1s3d}\rightarrow\underline{3p3d}+\underline{1s3d^2}\rightarrow\underline{3p3d^2}$. The values listed are the fit result. The intensity ratio of the two diagram lines was constrained to be equal to 0.51. I_{int} is the integrated intensity relative to that of the full spectrum. Units are given in parentheses.

Parameter		(a)	(b)	(c)	(d)	(e)	(f)
Shift $\underline{3p}$ (eV)	s_1	2.62	2.68	1.61	2.49	2.47	2.52
$\underline{3p3l}$	s_2	2.37	-1.88	-2.20	1.57	1.15	1.45
Width $\underline{3p_{3/2}}$(eV)	w_1	5.41	5.40	4.92	4.08	4.10	4.16
$\underline{3p_{1/2}}$	w_2	5.92	5.40	21.6	4.60	5.06	4.82
$\underline{3p3s}$	w_3		57.0				
$\underline{3p3p}$	w_4			5.0		14.4	
$\underline{3p3d}$	w_5				4.88	3.85	3.56
$\underline{3p3d^2}$	w_6						49.1
Intensity $\underline{3p_{3/2}}$ (Rel.)	a_1	0.997	0.983	0.970	0.969	1.000	0.989
$\underline{3p_{1/2}}$	a_2	0.470	0.502	0.112	0.439	0.413	0.436
$\underline{3p3s}$	a_3		0.008				
$\underline{3p3p}$	a_4			0.126		0.016	
$\underline{3p3d}$	a_5				0.065	0.052	0.061
$\underline{3p3d^2}$	a_6						0.002
Background (Rel.)	c_0	0.061	0.049	0.044	0.057	0.050	0.031
Background (10^{-5}/eV)	d_0	0.60	0.40	1.20	- 0.04	-0.06	-0.1
I_{int} $\underline{3p_{3/2}}$ (%)		66.2	58.4	50.5	49.0	49.2	42.8
$\underline{3p_{1/2}}$		33.8	29.8	25.8	25.0	25.0	21.8
$\underline{3p3s}$			11.8				
$\underline{3p3p}$				23.7		9.9	
$\underline{3p3d}$					26.0	15.9	14.7
$\underline{3p3d^2}$							20.7
R factor (%)	R_w	7.9	7.8	5.0	5.3	5.2	4.9
Goodness of fit	GoF	2.15	2.15	1.36	1.51	1.43	1.34

to the diagram lines, the only clear contribution is from the $\underline{3d}$ spectator hole spectrum.

The measured $K\beta$ line and the best theoretical fit (d) are plotted in Fig. 10. The fit quality, while reasonably good, is clearly inferior to that obtained for the $K\alpha$ spectrum. Although the differences between measured data and the fit are less than $\pm 3\sigma$ with most deviations less than $\pm 2\sigma$, systematic deviations are observed in particular near the positions of the β' and β_1'' satellites. A fit using the corresponding HF-calculated spectra shows a similar effect. Mathematically, the imperfect fit is due to the too large line spacing in the calculated $\underline{3d}$ spectator spectrum. A uniform reduction of the line spacing by 19% allows a much better fit, of the same high quality as that of $K\alpha$, with a GoF=0.91 and $R_w = 3.4\%$. Although this results in energy changes in the line positions which are of order of 1–2 eV at most, and hence of the order of the accuracy level of the calculations, we feel that without a sound physical reason such a uniform energy scale reduction can not be justified. Several attempts to obtain a more "compressed" calculated spectrum, including the addition of a $4s$ electron and a frozen-atom calculation, yielded only a marginal effect ($\leq$0.1 eV), and hence could not account for the observed effect. It is likely that the discrepancy is due to plasmon excitation or exchange interactions as discussed below.

4. Intensities and line widths

The linewidths and intensities obtained for the free-atom spectator hole best fit (d) in Table VII are given in Table VIII along with previous experimental measurements and theoretical predictions. Reasonable agreement is obtained with the previous x-ray measurements of LaVilla [15] although a simple addition of semi-empirical K widths with XPS-measured M widths tends to underestimate the $\underline{3p_{1/2}}$ width, as shown by the experimental entry listed under Yin.

The theoretical values of McGuire [49] are clearly much too large, as already observed by Yin *et al.* [50]. The reasonable agreement with the theoretical results of Yin *et al.* and the very good agreement with those of Crasemann and Chen [51], both of which are based on the free-atom calculation, indicates that although in a valence level, the $3p$ shell is localized well enough to allow treating the $K\beta_{1,3}$ transition as if occurring in a free atom, without interference from the solid's band structure.

Finally, although the intensity of the spectator spectrum is close to that obtained above for the $K\alpha$ line, and the expected shake-up and shake-off effects, no theoretical prediction is available for this specific quantity in the literature, to the best of our knowledge. Such calculations are highly desirable.

5. The origin of the β' line

In addition to free-atom multiplet splitting due to a $\underline{3d}$ spectator hole, as discussed above, several other sources were suggested for the β' line. The position and intensity of this line are compared with some of these predictions in Table IX and are discussed in this section.

Tsutsumi [7] suggested that the β' line in the iron group elements is due to a single, rather than two-electron transition but with an exchange interaction between the $\underline{3p}$ hole and the incomplete $3d$ shell. Within the HF theory, the resultant energy splitting is given by $\Delta E = (2S+1)[(2/15)G^1(3p,3d) + (3/35)G^3(3p,3d)]$, where S is the total spin of the $3d$ electrons and the G's are the Slater integrals. The relative intensity I'/I of the $K\beta'$ to the $K\beta_{1,3}$ is estimated from the multiplicity of the states yielding $I'/I = S/(S+1)$. This theory predicts ΔE in good agreement with experiment for almost all members of the iron-group elements, but greatly overestimates the intensities [9]. The last point is not surprising in view of the crude approximation involved. As the ground state

TABLE VIII. Linewidth (W) and integrated intensities (I) for the one- and two-hole components of the $K\beta$ spectrum. Present values are taken from fit (d) of Table VII. The intensity of the single-electron spectrum was taken as 100%.

		Experiment		Theory			
		Present	LaVilla[a]	Yin[b]	McGuire[c]	Yin[d]	CC[e]
W	$\underline{3p_{3/2}}$ (eV)	4.08	3.52[g]	2.48(30)	6.74	3.51	4.90
	$\underline{3p_{1/2}}$	4.60	3.52[g]	3.55(30)	6.74	3.51	5.00
	$\underline{3p_{3/2}3d}$	4.88 [f]					
	$\underline{3p_{1/2}3d}$	4.88 [f]					
I	$\underline{3p3d}$ (%)	35					

[a] Reference [15]. Fit to x-ray emission spectrum.
[b] Reference [50]. XPS-measured M width and semiempirical K width [54].
[c] K-level width taken from Ref. [38] and M-level widths taken from Ref. [49].
[d] K-level width taken from Ref. [38] and M-level widths taken from Ref. [50].
[e] K-level width of 1.44 eV and M-level widths of 3.56 and 3.46 eV for M_2 and M_3, respectively, from Ref. [51].
[f] A single width was used for all lines of the $\underline{3d}$ spectator transition.
[g] A single width was used for the $\underline{3p_{1/2,3/2}}$ lines.

TABLE IX. The energy shift ΔE from the peak of the $K\beta_{1,3}$ spectrum and the relative intensity of the β' line.

Source	ΔE (eV)	$I(\beta')/I(\beta_{1,3})$ (%)
Experimental		
Bearden[a] (1935)	8.3	1.3
Edamoto[b] (1950)	8.4	
Salem[c] (1976)	12.3(2.4)	6.2(2.0)
LaVilla[d] (1979)	8.4	
Present	8.4(6)	10.5(1.5)
Theoretical		
Salem[e] (1976)	0.0	0.0
Srivastava[f] (1982)	10.79	22.0
Present[g] S=1/2	6.8	33.3
[h] S=1	10.6	50.0

[a] Reference [40]. Determined from peak position of the feature.

[b] Reference [2]. Determined from the peak position of the feature.

[c] Reference [9]. Computer fit to emission data.

[d] Reference [15]. Feature's peak position.

[e] Reference [9]. Exchange interaction. HF calculations.

[f] Reference [8]. Plasmon theory.

[g] Assuming a $3p3d$ final hole configuration. HF calculation.

[h] Assuming a $3p3d^2$ final hole configuration. HF calculation.

$3d$ shell of copper is full, this theory predicts the absence of a $K\beta'$ line in copper, in obvious contradiction with experiment. However, if we assume the creation of one- and/or two-spectator holes, and the exchange interaction is assumed to occur between the (long-lived) $3d$ or $3d^2$ and the $3p$ holes in the final state, then the exchange interaction mechanism origin is possible for $K\beta'$ in copper as well. Using the Slater integrals calculated from the HF program of Froese Fischer [26] and a single $3d$ or a double $3d^2$ spectator hole, i.e., $S = 1/2$ or $S = 1$, we obtain the ΔE and intensity values listed in Table IX. As can be seen, ΔE is in reasonable agreement, particularly for the $3d$ spectator, while the relative intensity is, again, considerably overestimated. While for the $3d$ spectator our I'/I is almost twice as large as that of Salem, and hence closer to the theoretical value, the remaining discrepancy is still large, and a more refined calculation is required for comparison with the experimental results.

A different source for the $K\beta'$ line was suggested originally by Blochin [52] and further developed by Srivastava and co-workers [8]. This theory is based on the fact that the emitting atom is imbedded in a solid, and assumes that part of the energy of the $K\beta_{1,3}$ photon may be absorbed by the $3d$ electrons in the valence band giving rise to plasmon oscillations. This loss of energy will result in a satellite on the *low* energy side of the $K\beta_{1,3}$ line. As can be seen from Table IX, the predicted energy position is rather close to the measured value, and although the calculated intensity overestimates our measured value by a factor of 2, it is still closer than any of the other theoretical predictions. Again, more accurate calculations for copper and neighbouring atoms are called for.

V. CONCLUSIONS

The measurements of the $K\alpha_{1,2}$ and $K\beta_{1,3}$ spectra, presented here, which were measured by the same experimental setup, the resolution properties of which were well characterized and optimized, along with our extensive *ab initio* DF and HF calculation, result in a systematic and detailed description of these spectra and the underlaying processes.

The main conclusions and results of this study are as follows:

(a) A phenomenological, multi-Lorentzian representation is derived for both spectra. The measured $K\alpha_{1,2}$ spectrum is well represented by four symmetric Lorentzians, to an R factor of 1.3 %. The $K\beta_{1,3}$ spectrum, however, requires 5 Lorentzians for a similar representation, and yields an R factor of 1%. The fit results are in good agreement with previous, less accurate, studies. These phenomenological fits should prove useful for experiments where a simple analytic representation of the lines is required.

(b) Detailed fits of the measured spectra to DF and HF calculated diagram, one- and two-spectator hole transitions clearly show that the only appreciable contributions to the $K\alpha$ spectrum are the diagram and $3d$ spectator transitions. The same transitions account for the $K\beta$ spectrum as well. However, while for the $K\alpha$ the best fit yields a GoF=0.51 and an R factor of 3% and the fit residuals are random, the $K\beta$ fit is worse by a factor of two yielding an R factor of 5% and GoF=1.5 only, and fit residuals showing systematic deviations from the model.

(c) The measurements yield highly accurate values for the resolution corrected widths of the raw $K\alpha_{1,2}$ lines. The fits allow the separation of the widths and relative intensities of the various transitions.

(d) The fits indicate contributions of 26–30 % to both spectra from the $3d$ spectator transitions, and no contribution from $3s$ spectator ones. The $K\alpha$ spectrum may also include a small, ~0.5 %, contribution from the $3p$ spectator transition. No $3p$ spectator contribution can be separated out with any confidence for the $K\beta$ spectrum. Although there is some indication, in the form of a very small GoF reduction, for a contribution of the two-hole $3d^2$ spectator transition, this, again, can not be separated from the $3d$ spectator contribution with any confidence in both spectra.

(e) The systematic deviations in the $K\beta$ spectrum near the β' feature can be accounted for by assuming contributions from exchange interactions and/or plasmon excitations. A new exchange mechanism is suggested. The calculated energy positions due to both mechanisms are in good agreement with the measured data, although both overestimate the magnitude of the effect. No indication is found for any contribution of these processes to the $K\alpha$ spectrum.

Studies similar to those presented here for other mem-

bers of the iron group elements are required to explore the generality of the conclusions reached here. Accurate theoretical calculations of the expected cross sections for the various effects discussed here will allow a better understanding of the processes involved and are, therefore, also highly desirable. Finally, photoexcitation by synchrotron radiation of variable energy in the vicinity of the K edge will allow to turn on and off energetically some of the multielectronic excitations and other effects. The analysis of the resultant variation in the emission line shapes should prove a valuable tool in elucidating the contributions of the various processes to the line shape.

ACKNOWLEDGMENTS

We gratefully acknowledge valuable communications with B. Crasemann, University of Oregon, M. H. Chen, Lawrence Livermore National Laboratory, and P. Marketos, Oxford University. The expert programming assistance of G. Zipori at Bar-Ilan is also gratefully acknowledged. This work was partly supported by The Fund For Basic Research of The Israel Academy of Sciences, the Bar-Ilan University Research Authority, and the Bundesministerium für Forschung und Technologie under Contract No. 05 5SJAAI 7.

[1] A. Meisel, G. Leonhardt, and R. Szargan, *X-Ray Spectra and Chemical Binding* (Springer, New York, 1989).
[2] J. Edamoto, Rep. Res. Inst. Tohoku Univ. **A2**, 561 (1950).
[3] H. Sørum, J. Phys. F **17**, 417 (1987).
[4] J. Finster, G. Leonhardt, and A. Meisel, J. Phys. (Paris) **32**, C4-218 (1971).
[5] K. Tsutsumi and H. Nakamori, in *X-Ray Spectra and Electronic Structure of Matter*, edited by A. Faessler and G. Wiech (Fotodruck Frank OHG, München, 1973).
[6] L. G. Parratt, Rev. Mod. Phys. **31**, 616 (1959).
[7] K. Tsutsumi, J. Phys. Soc. Jpn. **14**, 1696 (1959); K. Tsutsumi, Y. Iwaskai, O. Aita, K. Ichikawa, and T. Watanabe, *ibid.* **47**, 1920 (1979).
[8] K. S. Srivastava *et al.*, Phys. Rev. A **19**, 4336 (1979); **25**, 2838 (1982).
[9] S. I. Salem, G. M. Hockney, and P. L. Lee Phys. Rev. A **13**, 330 (1976).
[10] J. Härtwig, G. Hölzer, E. Förster, K. Goetz, K. Wokulska, and J. Wolf, Phys. Status Solidi A **143**, 23 (1994).
[11] S. Doniach and M. Šunjić, J. Phys. C **3**, 285 (1970).
[12] W. C. Sauder, J. R. Huddle, J. D. Wilson, and R. E. LaVilla, Phys. Lett. **63A**, 313 (1977).
[13] M. Deutsch and M. Hart, Phys. Rev. B **26**, 5558 (1982).
[14] N. Maskil and M. Deutsch, Phys. Rev. A **37**, 2947 (1988).
[15] R. E. LaVilla, Phys. Rev. A **19**, 717 (1979).
[16] J. Bremer and H. Sørum, Phys. Lett. **75A**, 47 (1979).
[17] J. Härtwig, G. Hölzer, J. Wolf, and E. Förster, J. Appl. Crystallogr. **26**, 539 (1993).
[18] Although deconvolution is often used for this separation, one must bear in mind that representing the distortions due to the window function as a convolution is an approximation only, which may not be valid in all cases.
[19] W. H. Bragg and W. L. Bragg, *X-Rays and Crystal Structure* (Bell, London, 1915).
[20] S. Großwig, J. Härtwig, U. Alter, and A. Christoph, Cryst. Res. Technol. **18**, 501 (1983); S. Großwig, J. Härtwig, K.- H. Jäckel, R. Kittner, and W. Melle, Nauch. Apparat. **1**, 29 (1986).
[21] W. L. Bond, Acta Crystallogr. **13**, 814 (1960).
[22] J. Härtwig, S. Großwig, P. Becker, and D. Windisch, Phys. Status Solidi A **125**, 79 (1991).
[23] E. R. Cohen and B. N. Taylor, Rev. Mod. Phys. **59**, 1121 (1987); *Units of Measurement*, National Physical Laboratory Report, Teddington, UK, 1987.
[24] V. F. Miuskov, A. V. Mirenski, Y. N. Shilin, and N. G. Gasanov, Kristallografia **19**, 153 (1974) (in Russian).
[25] K. G. Dyall *et al.*, Compt. Phys. Commun. **55**, 425 (1989).
[26] C. Froese Fischer, Compt. Phys. Commun. **43**, 355 (1987).
[27] J. W. Cooper, Phys. Rev. A **38**, 3417 (1988); H. P. Saha, *ibid.* **42**, 6507 (1990); M.H. Chen, in *Atomic Inner Shell Physics*, edited by B. Crasemann (Plenum, New York, 1986).
[28] W. J. Kuhn and B. L. Scott, Phys. Rev. A **34**, 1125 (1986); B. L. Scott, *ibid.* **34**, 4438 (1986).
[29] E. U. Condon and G. H. Shortley, *The Theory of Atomic Spectra* (Cambridge, Cambridge, U.K., 1951).
[30] J. C. Slater, *Quantum Theory of Atomic Structure* (McGraw-Hill, New York, 1960), Vol. II, App. 21.
[31] R. D. Cowan, *The Theory of Atomic Structure and Spectra* (University of California, Berkeley, 1981), App. I.
[32] P. H. Citrin, P. M. Eisenberger, W. C. Marra, T. Åberg, J, Utriainen, and E. Kaellne, Phys. Rev. B **10**, 1762 (1974).
[33] J. Ayers and J. Ladell, Phys. Rev. A **37**, 2404 (1988).
[34] P. L. Lee and S. I. Krause, Phys. Rev. A **10**, 2027 (1974).
[35] J. Kawai *et al.*, Solid State Commun. **70**, 567 (1989).
[36] J. C. Fuggle and S. F. Alvarado, Phys. Rev. A **22**, 1615 (1980).
[37] L. I. Yin, I. Adler, M. H. Chen, and B. Crasemann, Phys. Rev. A **7**, 897 (1973).
[38] M. H. Chen, B. Crasemann, and H. Mark, Phys. Rev. A **21**, 436 (1980).
[39] H. Berger, X-Ray Spectrom. **15**, 241 (1986). We corrected the values in his Table 1 for the width of the reflection curve as discussed by the author.
[40] J. A. Bearden and C. H. Shaw, Phys. Rev. **48**, 18 (1935); J. Ladell, W. Parish, and J. Taylor, Acta Crystallogr. **12**, 561 (1959).
[41] Y. Cauchois and C. Senemaud, *Wavelengths of X-Ray Emission Lines and Absorption Edges* (Pergamon, Oxford, 1978). Based on measurements by Bearden and Shaw [40], Y. Cauchois, C. R. Acad. Sci. (Paris), **201**, 1359 (1935) and T. Hayasi, Sci. Rep. Tohoku Univ. Ser. I **36**, 225 (1952).
[42] J. R. Cuthill and E. N. Erickson, private communication, as cited in Ref. [46].
[43] K. N. Huang, M. Ayogi, N. H. Chen, B. Crasemann, and H. Mark, At. Data Nucl. Data Tables **18**, 243 (1976).
[44] U. D. Misra, M. Sah, and B. G. Gokhale J. Phys. B **25**, 4107 (1992).
[45] H. H. Madden, D. M. Zehner, and J. R. Noonan, Phys. Rev. B **17**, 3074 (1978).
[46] A. J. McAlister *et al.*, Phys. Rev. B **12**, 2973 (1975).
[47] P. Marketos, private communication.
[48] J. H. Scofield, At. Data Nucl. Data Tables **14**, 121 (1974);

in *Atomic Inner-shell Processes*, edited by B. Crasemann (Academic, New York, 1975), Vol. I, p. 265.
[49] E. J. McGuire, Phys. Rev. A **5**, 1043 (1972).
[50] L.I. Yin, I. Adler, T. Tsang, M. H. Chen, D. A. Ringers, and B. Crasemann, Phys. Rev. A **9**, 1070 (1974).
[51] B. Crasemann and M.H. Chen, private communication.
[52] M. A. Blochin, *Physik der Röntgenstrahlen* (Verlag Technik, Berlin, 1957), p. 343.
[53] V. M. Pessa, X-Ray Spectrom. **2**, 169 (1973). This is a resolution corrected, critical evaluation of results by six earlier groups including Bearden and Shaw [40].
[54] M. O. Krause and J. H. Oliver, J. Phys. Chem. Ref. Data **8**, 329 (1979).
[55] M. H. Chen, B. Crasemann, and H. Mark, Phys. Rev. A **24**, 177 (1981).
[56] J. A. Bearden, Rev. Mod. Phys. **39**, 78 (1967).
[57] R. Bruhn, B. Sontag, and H. W. Wolf, J. Phys. B **12**, 203 (1979).
[58] J. C. Fuggle and W Martensson, J. Electron. Spectrosc. **21**, 275 (1980).
[59] F. Herman and S. Skilman, *Atomic Structure Calculations* (Prentice Hall, Englewood Cliffs, N.J., 1963).